Journal of Civil Engineering and Urban Planning (2024)
Clausius Scientific Press, Canada

DOI: 10.23977/jceup.2024.060309
ISSN 2616-3969 Vol. 6 Num. 3

Characterization of dynamic response of buried circular pipeline under the action of cylindrical SH wave

Siqin Wang, Shiwei Lu*, Shun Yi, Ruizhe Sun

School of Urban Construction, Yangtze University, Jingzhou, China
**Corresponding author: lushiwei364@163.com*

Keywords: Cylindrical SH waves, Dynamic Stress Concentration Factor, Single-line pipe, Inner wall of pipe, Wave source location

Abstract: To assess the stability of transportation pipelines during blasting excavation, this study investigates the dynamic response of buried circular pipelines under cylindrical SH waves. The research analyzes the distribution pattern of the Dynamic Stress Concentration Factor. For a single pipeline, when the number of virtual source points and stress monitoring points respectively reaches 50 and 60, it meets the requirements of further analysis. If the distance between the wave source and the pipeline axis doesn't less than 5 times the outer diameter of pipeline, the Dynamic Stress Concentration Factor of the soil and the inner wall of the pipeline basically don't change.

1. Introduction

With the continuous development of society, surface transportation has gradually become unable to meet the current transportation needs, so the development and utilization of underground space has become particularly important. The destructive power of earthquake and blasting engineering is enormous, which has a significant impact on the safety of underground engineering. Scientific exploration and discussion of it will contribute to the healthy, rapid, and high-quality development of the industry. Therefore, it has profound significance to study the dynamic response of buried pipelines under stress waves for determining the safe state of normal use and bearing capacity of pipeline transportation engineering.

In most studies on SH waves, some scholars overlook the discontinuity of displacement at the pipe-soil interface when discussing the dynamic response of SH waves to pipelines. Therefore, this article uses the Indirect Boundary Integral Equation Method (IBIEM) to analyze a single buried pipeline, taking the Dynamic Stress Concentration Factor as the research object to obtain the analytical solution of IBIEM. It analyzes the dynamic response of a single buried pipeline under the action of cylindrical SH waves. And explores the influencing factors and variation patterns of the dynamic response of a single buried pipeline under different parameter conditions, and identifies the weak areas of the pipeline under the influence of cylindrical SH waves. Then lay the foundation for future theoretical research[1-3].

2. Simplified calculation model and wave field analysis

As shown in Fig. 1, in the fully elastic spatial domain, a cylindrical SH wave is generated at a blasting point on the left side of the buried pipeline, with the wave source position O_1 on the same line as the pipeline center O_2. To avoid singularity in the calculation results, virtual wave sources S_1 and S_2 are placed inside the tunnel, and S_3 is placed outside the pipeline. Virtual wave sources S_1 and S_2 propagate towards the soil outside the pipeline, while virtual wave source S_3 propagates towards the inside of the pipeline.

For elastic wave problems, the total wave field can be decomposed into a free field and a scattering field. For a single pipeline in a fully elastic spatial domain, with an inner radius of a_1 and an outer radius of a_2, the distance from the wave source to the center of the pipeline is d. The coordinate of the wave source is (x_0, y_0). The indirect boundary integral equation method (IBIEM) is used to analyze it. The IBIEM constructs the scattered wave field from the virtual wave sources distributed at or near the boundary. The source density is solved by the boundary conditions, and then the total response is obtained. In addition to the advantages of the general boundary element method, IBIEM also has the following two characteristics: (1) The position of the wave source is not defined on the irregular interface, but defined at a certain distance away from the irregular interface. The position of the observation point and the position of the wave source will not coincide, which can avoid the need to deal with the problem of integral singularity in the general boundary element method. (2) The main feature of the wave source method is that the discrete wave source is used to replace the continuous wave source, and the sum operation of the wave source is used to replace the integral operation, which simplifies the calculation method. Assuming that the virtual wave source in the fully elastic spatial domain is S_1, in a single pipeline is S_2. And the coordinates of the discrete points of S_1 and S_2 are (x_i, y_i). Their discrete number are both M (assuming S_1 and S_2 coincide). The coordinates of the discrete points of virtual wave source S_3 outside the pipeline are (x_k, y_k), and the discrete number of S_3 is N. The number of observation points on the inner surface and the outer surface of the pipeline are respectively L_1 and L. Assuming that $L_1=L$, $L>M$, $L>N$, and the coordinates of the observation points are (x_j, y_j).

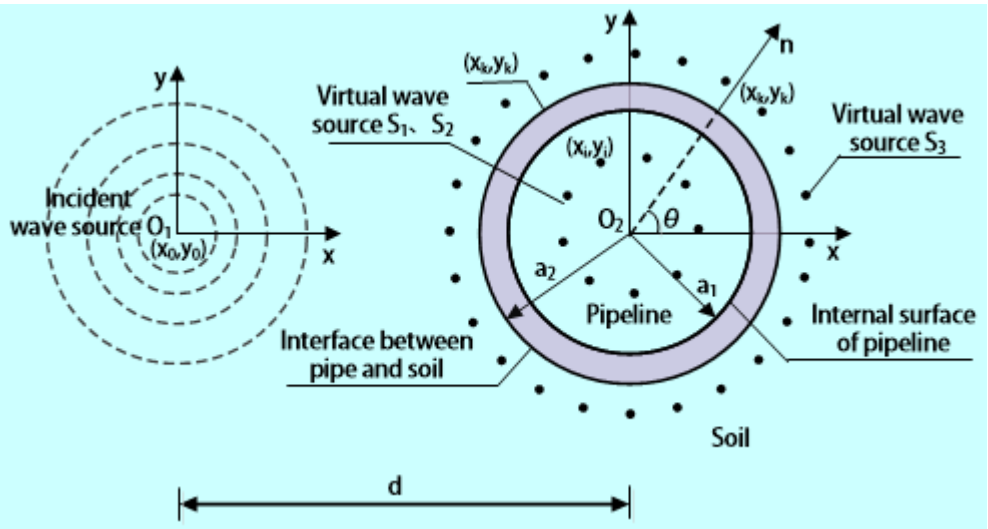

Figure 1: Calculated working conditions of single-line circular pipe

(1) Free field

Due to the fact that the calculation condition is in a fully elastic spatial domain in a free field, only incident waves exist in the free field.

The displacement of the incident wave can be expressed as:

$$W^{(\mathrm{i})} = \mathrm{H}_0^{(1)}(k_1 r_{0j}) \tag{1}$$

$$k_1 = \frac{2\pi f}{c_s} \tag{2}$$

$$r_{0j} = \sqrt{(x_j - x_0)^2 + (y_j - y_0)^2} \tag{3}$$

where k_1 is the number of waves in the fully elastic spatial domain, f is the frequency of the incident wave, and c_s is the wave velocity. H_0 is the zero order Hankel function, which physically represents the cylindrical wave source function.

The total free wave field:

$$W^{(\mathrm{f})} = \mathrm{H}_0^{(1)}(k_1 r_{0j}) \tag{4}$$

The shear stress caused by the corresponding free field can be expressed as:

$$\tau_{xz}^{(\mathrm{f})} = \mu_1 \frac{\partial W}{\partial x} = \mu_1 \frac{x_j - x_0}{r_{0j}} [-k_1 \mathrm{H}_1^{(1)}(r_{0j})] \tag{5}$$

$$\tau_{xz}^{(\mathrm{f})} = \mu_1 \frac{\partial W}{\partial y} = \mu_1 \frac{y_j - y_0}{r_{0j}} [-k_1 \mathrm{H}_1^{(1)}(r_{0j})] \tag{6}$$

where μ_1 is the shear modulus of soil in the fully elastic spatial domain.

(2) Scattered field

In pipelines in the fully elastic spatial domain, scattered waves can be constructed by virtual wave source surfaces S_1, S_2, and S_3.

The displacement of the scattered wave field can be expressed as:

$$\begin{aligned} W^{(\mathrm{s}_1)} &= \sum_{i=1}^{\mathrm{M}} A_i \mathrm{H}_0^{(1)}(k_1 r_{ij}) \\ W^{(\mathrm{s}_2)} &= \sum_{i=1}^{\mathrm{M}} B_i \mathrm{H}_0^{(1)}(k_2 r_{ij}) \\ W^{(\mathrm{s}_3)} &= \sum_{k=1}^{\mathrm{N}} C_k \mathrm{H}_0^{(1)}(k_2 r_{kj}) \end{aligned} \tag{7}$$

where k_2 is the wave number in the pipeline, distinguished from k_1. A_i, B_i, and C_k are the wave source density on the boundary of the virtual wave source surface.

The shear stress caused by scattering field can be expressed as:

Shear stress generated by S_1:

$$\tau_{xz}^{(\mathrm{s}_1)} = \mu_1 \frac{\partial W}{\partial x} = \mu_1 \sum_{i=1}^{M} A_i \frac{x_j - x_i}{r_{ij}} [-k_1 \mathrm{H}_1^{(1)}(r_{ij})] \tag{8}$$

$$\tau_{yz}^{(s_1)} = \mu_1 \frac{\partial W}{\partial y} = \mu_1 \sum_{i=1}^{M} A_i \frac{y_j - y_i}{r_{ij}} [-k_1 \mathrm{H}_1^{(1)}(r_{ij})] \tag{9}$$

Shear stress generated by S_2:

$$\tau_{xz}^{(s_2)} = \mu_2 \frac{\partial W}{\partial x} = \mu_2 \sum_{i=1}^{M} B_i \frac{x_j - x_i}{r_{ij}} [-k_2 \mathrm{H}_1^{(1)}(r_{ij})] \tag{10}$$

$$\tau_{yz}^{(s_2)} = \mu_2 \frac{\partial W}{\partial y} = \mu_2 \sum_{i=1}^{M} B_i \frac{y_j - y_i}{r_{ij}} [-k_2 \mathrm{H}_1^{(1)}(r_{ij})] \tag{11}$$

Shear stress generated by S_3:

$$\tau_{xz}^{(s_3)} = \mu_2 \frac{\partial W}{\partial x} = \mu_2 \sum_{i=1}^{N} C_k \frac{x_j - x_k}{r_{kj}} [-k_2 \mathrm{H}_1^{(1)}(r_{kj})] \tag{12}$$

$$\tau_{yz}^{(s_3)} = \mu_2 \frac{\partial W}{\partial y} = \mu_2 \sum_{i=1}^{N} C_k \frac{y_j - y_k}{r_{kj}} [-k_2 \mathrm{H}_1^{(1)}(r_{kj})] \tag{13}$$

where μ_2 is the shear modulus of the pipeline.

According to the calculation requirements, the calculated wave field is divided into fully elastic spatial domain and pipeline internal wave field. From the analysis, it can be seen that in the fully elastic spatial domain, the wave field is generated by the incident wave and the virtual wave source surface S_1. Therefore:

$$W^R = W^{\mathrm{f}} + W^{s_1} \tag{14}$$

$$\tau^R = \tau^{\mathrm{f}} + \tau^{s_1} \tag{15}$$

The wave field inside the pipeline is composed of virtual wave source surfaces S_2 and S_3:

$$W^P = W^{s_2} + W^{s_3} \tag{16}$$

$$\tau^P = \tau^{s_2} + \tau^{s_3} \tag{17}$$

where W^P is the total displacement inside the pipeline, and W^R is the total displacement inside the soil. τ^P is the sum of the shear stresses inside the pipeline, and τ^R is the sum of shear stresses in the soil.

2.1 Analytical solution considering interface effects between pipelines and soil

In practical engineering, the displacement between pipelines and soil is usually not continuous. So in calculation, it is necessary to consider the situation of discontinuous displacement at the pipe-soil interface. Therefore, the parameter *Kr* (stiffness coefficient of the spring at the pipe-soil interface) is introduced, and the boundary condition is obtained based on Hooke's law analysis:

$$\begin{cases} \tau_{rz}^{R} = \tau_{rz}^{P} & r = a_2 \\ \tau_{rz}^{s_2} + \tau_{rz}^{s_3} = 0 & r = a_1 \\ W^{R} - W^{P} = \dfrac{\tau_{rz}^{R}}{K_r} & r = a_2 \end{cases} \tag{18}$$

Represent it in matrix form as:

$$\begin{pmatrix} -\tau^{(s_1)'} & \tau^{(s_2)'} & \tau^{(s_3)'} \\ 0 & \tau^{(s_2)'} & \tau^{(s_3)'} \\ W^{(s_1)'} - \dfrac{\tau^{(s_1)'}}{K_r} & -W^{(s_2)'} & -W^{(s_3)'} \end{pmatrix} \begin{pmatrix} A_i \\ B_i \\ C_k \end{pmatrix} = \begin{pmatrix} \tau^{(f)} \\ 0 \\ \dfrac{\tau^{(f)}}{K_r} - W^{(f)} \end{pmatrix} \tag{19}$$

To facilitate analysis and obtain general conclusions, this article defines the dynamic stress concentration coefficient DSCF:

$$DSCF = \left| \frac{\tau_{\theta z}}{\mu k H_1^{(1)}(kr)} \right| \tag{20}$$

in which,

$$\tau_{\theta z} = -\tau_{xz}\sin\theta + \tau_{yz}\cos\theta \tag{21}$$

where $\tau_{\theta z}$ is the circumferential shear stress, θ is the angle between the normal vector of the boundary point of the cave and the x and y axes, μ is the shear modulus of the soil, k is the wave number of the soil, and r is the distance from the wave source to the monitoring point.

2.2 Method feasibility verification

In order to make the calculation results closer to actual engineering, the interface effect of the pipe and soil is considered. The stiffness coefficient is set as K_r. According to the above equation, when K_r approaches infinity, the pipe-soil interface is equivalent to a rigid one. To verify the feasibility of this method, K_r is set to approach 10^8, and the incident wave frequency is 100 Hz. The outer diameter of the pipeline is 1.02 m, the inner diameter is 1.0 m, and the wave source coordinates are (-60, 0). Other parameters are shown in Table 1. The feasibility of this calculation method is verified by comparing the DSCF of soil and pipeline inner walls with that without considering interface effects. The calculation results are shown in Fig. 2 and Fig. 3.

Table 1: Table of parameters of research subjects

Material category	Density ρ (kg/m^3)	Poisson's ratio	K_r	Frequency f
Pipeline	2780	0.3	$K_r \rightarrow 10^8$	100Hz
Soil mass	1930	0.35		

By comparing the DSCF distribution curves in soil and pipeline inner walls, it was found that considering interface effects, when K_r is approach to 10^8, the DSCF distribution curve basically coincides with that of the calculation method without considering interface effects. This indicates that the calculation method considering interface effects is in line with the calculation results, with high accuracy and strong feasibility, and can be used as a basic method for dynamic response analysis of pipe and soil[4-6].

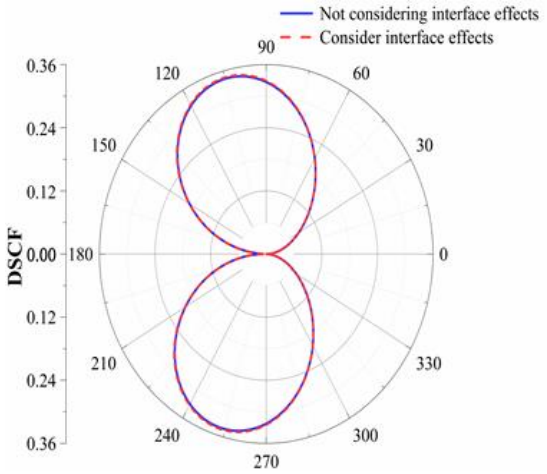

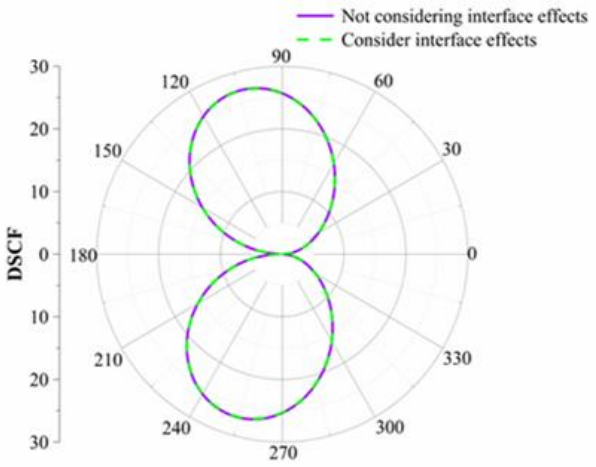

Figure 2: Comparison chart of feasibility analysis in soil (Left)

Figure 3: Comparative analysis of the feasibility of the inner wall of the pipe (Right)

3. Example analysis and discussion

3.1 Calculated operating conditions

Wuhan is located in the middle and lower reaches of the Yangtze River, with the upper soil mainly composed of clay. Taking a buried pipeline in the urban area of Wuhan as the engineering background, dynamic response analysis is conducted on it. According to relevant information, the buried pipeline is a commonly used large diameter ductile iron pipeline with an inner diameter of 1 m, an outer diameter of 1.02 m, and a wall thickness of 0.01 m. The soil around the pipeline is composed of silty clay, and the research object parameters are shown in Table 2.

Table 2: Table of pipeline and soil parameters

Material category	Density ρ (kg/m^3)	Poisson's ratio	Shear modulus μ (Pa)
Buried pipeline	$2.78*10^3$	0.3	$7.5*10^9$
Solum	$1.93*10^3$	0.35	$5.0*10^7$

3.2 The Influence of Discrete Number of Virtual Wave Sources and Monitoring Points on Calculation Accuracy

According to literature and extensive numerical calculations, it has been found that different values of virtual wave source radius a_i, a_k (the wave source radius with a_i being S_1 and S_2, and a_k being S_3), and L, M, and N (making M=N for simplified calculations) all have varying degrees of impact on the accuracy of the calculation. To obtain the optimal calculation results, the discrete numbers M and N (M=N) of the virtual wave source and the number of monitoring points L are discussed. a_i=0.3a,a_k=1.16a,Kr = $n\mu_1/a_2$,Take n=0.1, k_1a_2=0.1, and the wave source coordinate is (-60,0). Other

parameters are defined according to the parameter table in the calculation conditions, as shown in Table 2. The error analysis of the discrete number of different virtual wave sources and the number of monitoring points are shown in Table 3.

After extensive data analysis, it can be concluded that the optimal exact solution can be obtained when a_i=0.7a, a_k=1.54a, M=N=50, and L=60. The calculation error in the soil is 8.80*10$^{-10,}$ and in the pipeline inner wall is 5.65*10^{-10}, both of which meet the calculation accuracy requirements (1*10^{-4}). It can provide high calculation accuracy for later analysis. The configuration parameters with small errors and the selection basis for the virtual wave source radius lay a scientific and effective theoretical foundation for the parameter selection of dynamic response analysis of single line pipelines, making the analysis results more accurate and effective[7-8].

Table 3: Analysis table of monitoring points and discrete points taking values

Discrete number N(M)	Monitoring points L	Ratio L/M	Internal error value of soil	Error value of pipeline inner wall
200	600	3	1.06*10^{-6}	1.07*10^{-6}
240	600	2.5	5.35*10^{-7}	5.46*10^{-7}
250	500	2	9.37*10^{-7}	9.17*10^{-7}
200	300	1.5	3.44*10^{-7}	3.49*10^{-7}
20	60	3	2.21*10^{-7}	4.41*10^{-7}
24	60	2.5	9.60*10^{-9}	2.36*10^{-8}
30	60	2	1.07*10^{-9}	3.34*10^{-9}
40	60	1.5	7.83*10^{-10}	7.44*10^{-10}
50	60	1.2	8.80*10^{-10}	5.65*10^{-10}
10	20	2	0.44*10^{-2}	0.62*10^{-2}
6	9	1.5	0.28*10^{-2}	0.32*10^{-2}

3.3 Parameter Discussion

Table 4: Single-line pipeline calculation working conditions table

Wave source distance D(m)	ka_2	Stiffness K_r	Wave source distance D(m)	ka_2	Stiffness K_r
D=5a_2 (outside diameter)	ka_2=0.1	K_r=0.1μ_1/a_2	D=100a_2 (outside diameter)	ka_2=0.1	K_r=0.1μ_1/a_2
		K_r=1μ_1/a_2			K_r=1μ_1/a_2
		K_r=10μ_1/a_2			K_r=10μ_1/a_2
	ka_2=0.5	K_r=0.1μ_1/a_2		ka_2=0.5	K_r=0.1μ_1/a_2
		K_r=1μ_1/a_2			K_r=1μ_1/a_2
		K_r=10μ_1/a_2			K_r=10μ_1/a_2
	ka_2=1.0	K_r=0.1μ_1/a_2		ka_2=1.0	K_r=0.1μ_1/a_2
		K_r=1μ_1/a_2			K_r=1μ_1/a_2
		K_r=10μ_1/a_2			K_r=10μ_1/a_2
D=5a_2 (outside diameter)	ka_2=2.0	K_r=0.1μ_1/a_2	D=100a_2 (outside diameter)	ka_2=2.0	K_r=0.1μ_1/a_2
		K_r=1μ_1/a_2			K_r=1μ_1/a_2
		K_r=10μ_1/a_2			K_r=10μ_1/a_2

Based on the above analysis and discussion of calculation accuracy and verification of the feasibility of the method, in order to obtain general conclusions, parameter analysis is conducted on the calculation condition. For the convenience of analysis, the following dimensionless parameters

are defined, ka2(k is the wave number inside the soil and k=k1, which is related to the wave velocity cs and the incident wave frequency f).The definition of ka2 can be transformed into a discussion of the frequency of the incident wave, and k2 can be represented as k2=k1cs1/cs2. ka2 is taken as 0.1, 0.5, 1.0, and 2.0 respectively, and Kr is defined Kr = nμ1/a2(μ1 is the shear modulus of the soil), where n is taken as 0.1, 1, and 10 respectively for discussion. On this basis, two types of wave source distances are discussed (establishing numerical relationships with a2), taking 5a2 and 100a2 respectively. The radius of the virtual wave source, the number of discrete virtual wave sources, and the number of detection points are taken as ai=0.7a, ak =1.54a, M=N=50, and L=60 according to the optimal solution. The specificworking conditions and related parameters are shown in Table 4.

4. Numerical Results and Discussion

4.1 The effect of Kr on the Circumferential Distribution of DSCF in Soil

For the dynamic response of the soil at the pipe-soil interface under the action of cylindrical SH waves, a monitoring radius of $a=a_2$ is taken as the research object, and the circumferential distribution of the DSCF is shown in Fig. 4.

From Fig. 4, it can be seen that when $D=5a_2$ and ka_2 take the above values, the DSCF circumferential distribution curve is axisymmetric about 0~π. And at the same angle θ, the larger n (K_r), the smaller its DSCF value. From this analysis, it can be seen that in the soil at the pipe-soil interface, when $D=5a_2$, the maximum values of DSCF are distributed between π/3-2 π/3 and 4 π/3~5 π/3 with changes in ka_2 and K_r. While the minimum values are all in the range of 0 and π, and are infinitely close to 0.When $K_r \rightarrow 10^8$, the DSCF value is smaller at the same angle θ. From this, it can be seen that the interface stiffness coefficient K_r has a significant impact on the calculation results of DSCF.

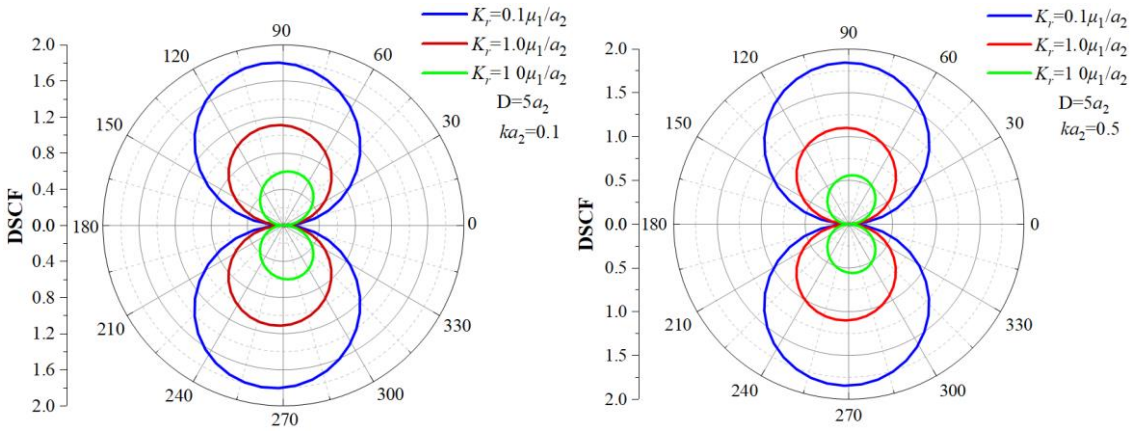

(a) ka2=0.1 (b) ka2=0.5

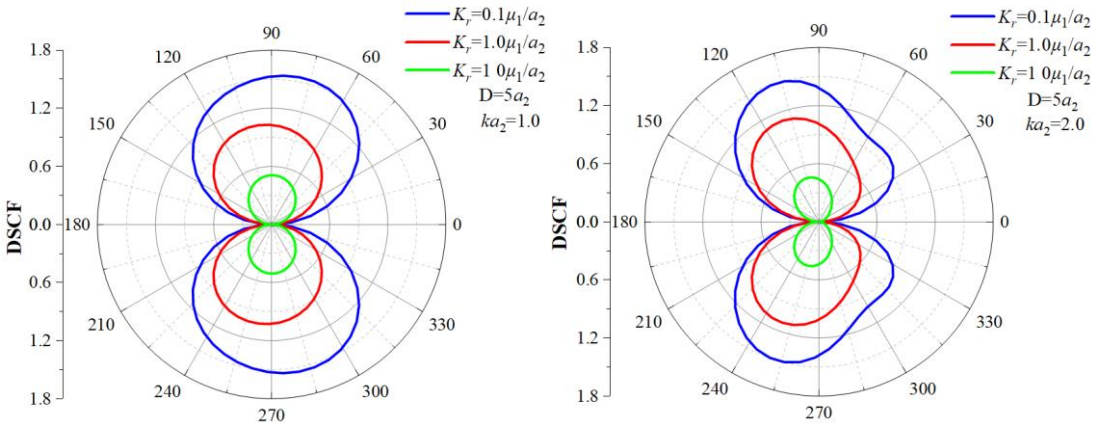

(c) ka2=1.0 (d) ka2=2.0

Figure 4: Circumferential distribution curves of DSCF within the soil for D=5a_2 at different ka_2

From Fig. 5, it can be seen that when D=100a_2, the circumferential distribution of DSCF is basically the same as when D=5a_2. From this, we can know that both the stiffness coefficient K_r and the incident wave frequency f (ka_2) have a significant impact on the calculation results, while the influence of the wave source distance D on the numerical value of DSCF is not significant.

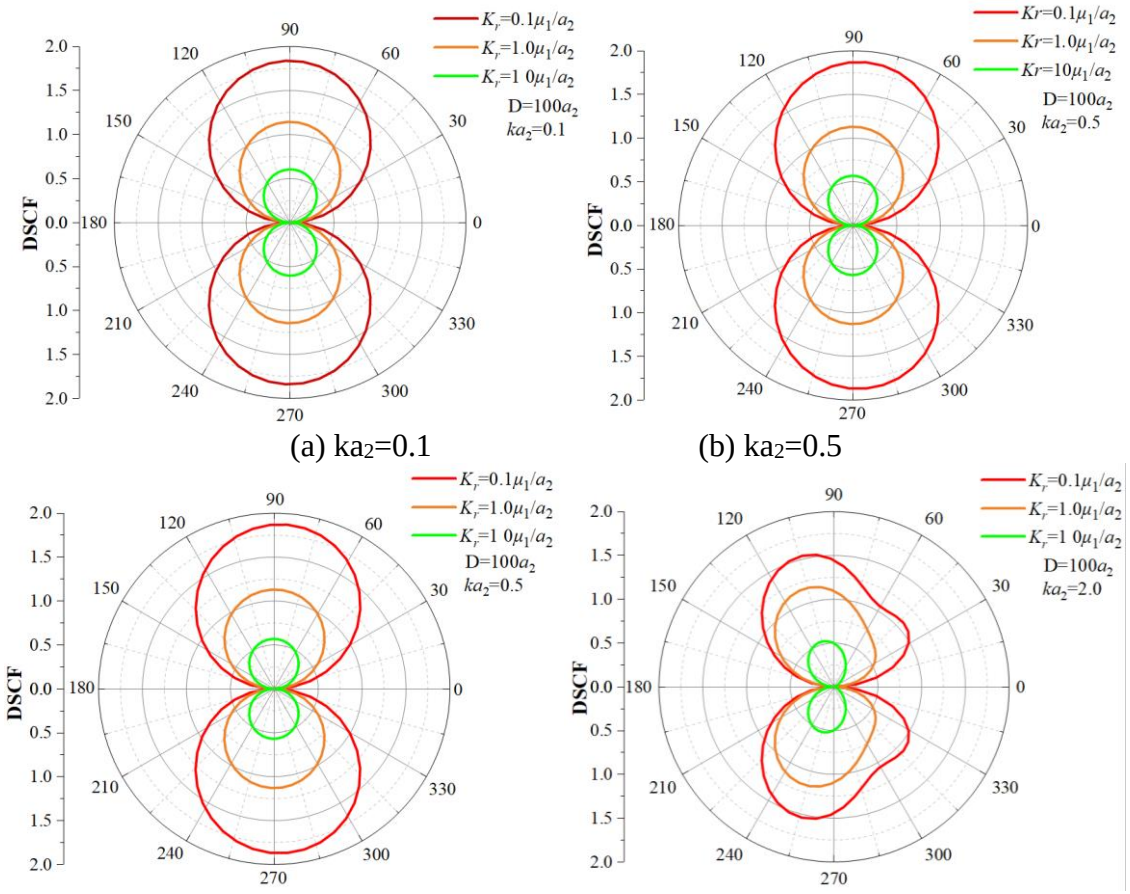

(a) ka2=0.1 (b) ka2=0.5

(c) ka2=1.0 (d) ka2=2.0

Figure 5: Circumferential distribution curve of DSCF in soil at D=100a_2 with different ka_2

4.2 The effect of Kr on the circumferential distribution of DSCF on the inner wall of pipelines

For the dynamic response of the inner wall of the pipeline under the action of cylindrical SH waves, a monitoring radius of $a=a_1$ (inner wall of the pipeline) is taken as the research object, and the circumferential distribution diagram of the DSCF is shown in Fig. 6.

From Fig. 6, it can be seen that when $D=5a_2$ and ka_2 take the above values, the DSCF circumferential distribution curve is axisymmetric about 0~π. And at the same angle θ, the larger n (K_r), the greater its DSCF value. And the interface stiffness coefficient K_r has a greater impact on the numerical value of DSCF compared to that in soil, and the trend of change is opposite. From this analysis, it can be seen that in the inner wall of the pipeline, when $D=5a_2$, the peak values of DSCF are distributed within the range of π/2-2 π/3 and 4 π/3-3 π/2 with changes in ka2 and Kr. While the minimum values of DSCF are all in the range of 0 and π, infinitely close to 0. When $K_r \rightarrow 10^5$, the DSCF value is larger at the same angle θ. This is opposite to the trend of changes in the soil mass. Therefore, it can be concluded that the stiffness coefficients K_r and ka_2 have a significant impact on the calculation results of DSCF. Compared with the DSCF curve in the soil, it was found that the DSCF value on the inner wall of the pipeline is much greater in numerical terms than that in the soil. Therefore, the inner wall of the pipeline is more prone to damage under the action of cylindrical SH waves, and the distribution area is concentrated between π/2-2 π/3 and 4 π/3-3 π/2. So this interval should be a key monitoring area for the inner wall of the pipeline.

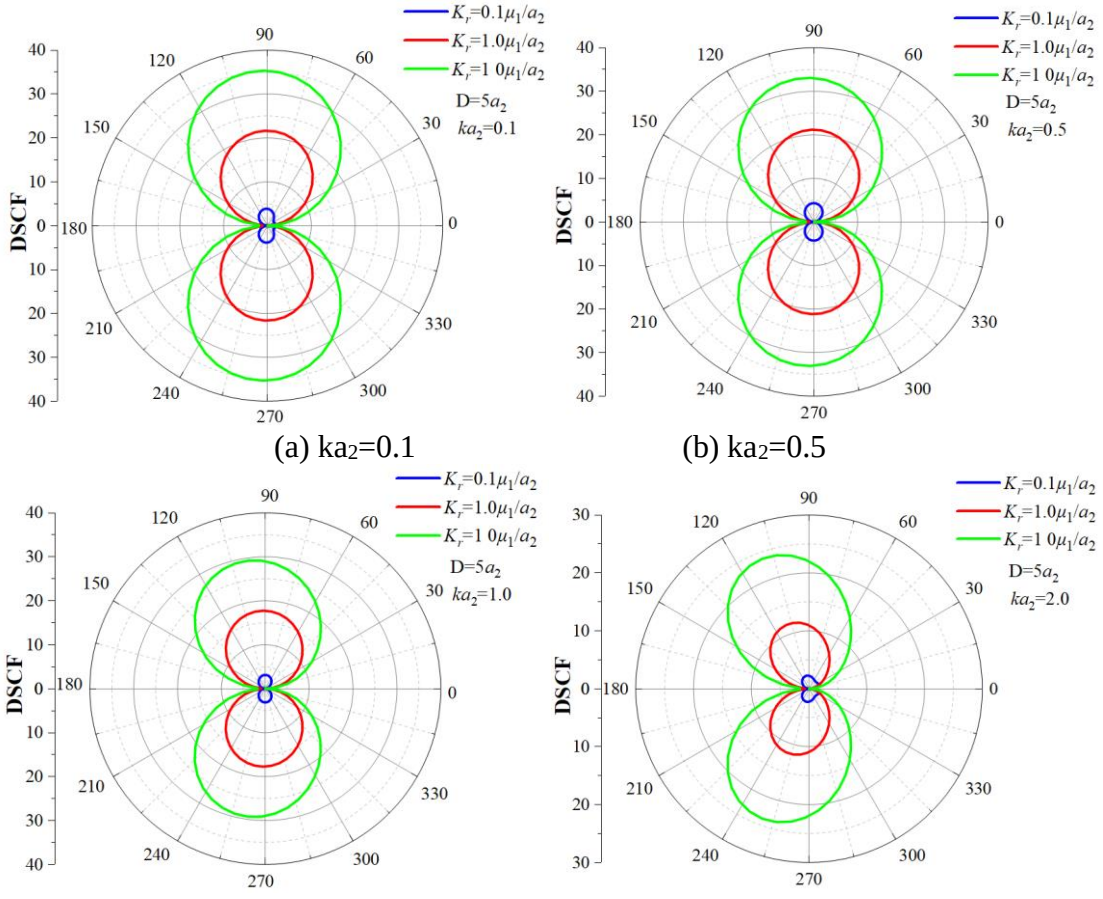

(a) ka2=0.1 (b) ka2=0.5

(c) ka2=1.0 (d) ka2=2.0

Figure 6: Curve of circumferential distribution of DSCF in the pipe at $D=5a_2$ with different ka_2

From Fig. 7, it can be seen that when $D=100a_2$, the circumferential distribution of DSCF is basically the same as when D=5a_2.It shows that regardless of the value of D, the maximum dynamic

stress concentration coefficient is distributed within the range of π/2-2 π/3 and 4 π/3-3 π/2. Compared to the soil, the DSCF value on the inner wall of the pipeline is larger and the distribution range is more concentrated. Moreover, as ka_2 increases, its peak value of DSCF decreases. From this, it can be seen that under the action of cylindrical SH waves, different values of D will have a certain impact on the shape and numerical value of the DSCF distribution curve. Compared to the dynamic response in the soil, the inner wall of the pipeline is more susceptible to damage. So the analysis of the inner wall of the pipeline is more important[9-10].

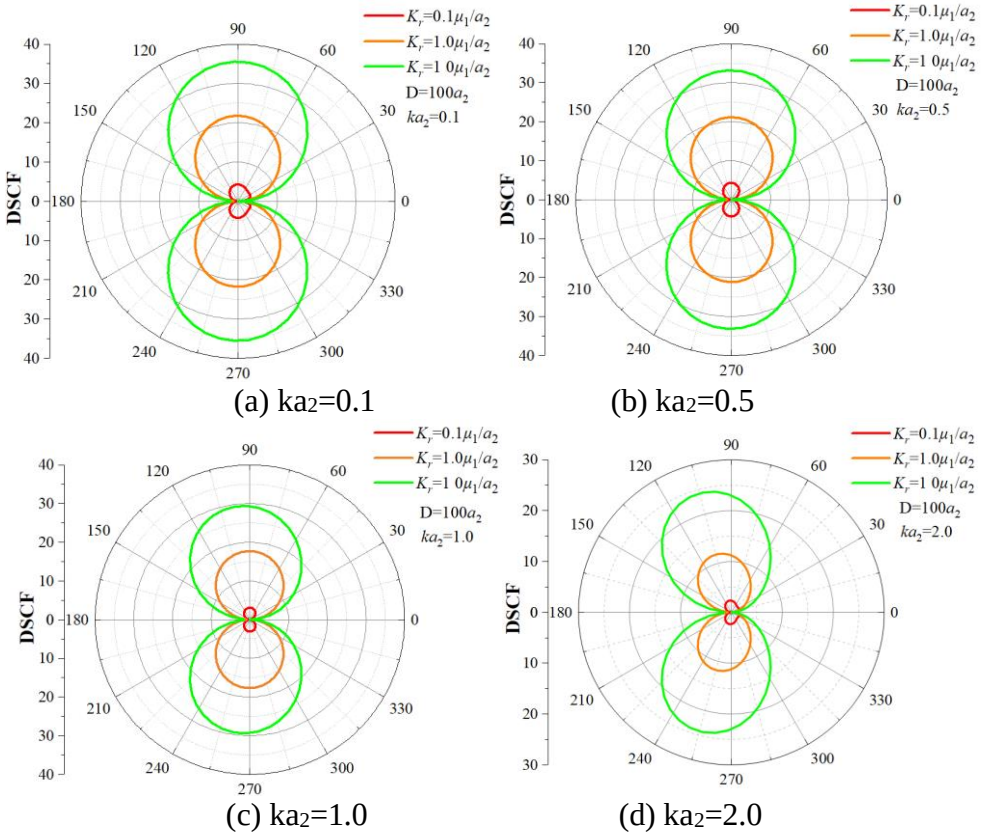

(a) ka_2=0.1 (b) ka_2=0.5

(c) ka_2=1.0 (d) ka_2=2.0

Figure 7: Circumferential distribution curve of DSCF in the pipe at D=100a_2 with different ka_2

4.3 The effect of different ka on the peak value of DSCF in soil

From the above results, it can be seen that the frequency of the incident wave has a significant impact on the distribution pattern and maximum value of DSCF. Therefore, the parameters related to the frequency of the incident wave (ka_2) are analyzed and discussed. The trend of the maximum DSCF value with ka_2 under certain other operating conditions is shown in Fig. 8.

From Fig. 8, it can be observed that when D=5a_2 and D=100a_2, the trend of the DSCF peak curve with ka_2 is basically the same. In terms of numerical value, the larger the stiffness coefficient K_r, the smaller the peak value of its DSCF. When K_r=0.1μ_1/a_2, as ka_2 increases, the peak value of DSCF first increases and then decreases at 0.1<ka_2<1.25, and gradually increases again at ka_2>1.25. When K_r=1.0μ_1/a_2, the trend of the curve is relatively flat, and the peak value of DSCF remains stable between 1.0 and 1.2.When K_r=10μ_1/a_2, the trend of the curve changes as ka_2 increases, slowly decreasing at 0.1<ka_2<1.25, and tending towards DSCF=0.5 at ka_2>1.25. From this, it can be seen that the impact of incident wave frequency f on the peak value of DSCF varies in degree under different stiffness coefficients K_r. When the stiffness coefficient K_r is small, the impact on its DSCF peak is more significant. The larger the interface stiffness coefficient K_r, the smaller the DSCF value

of the soil around the pipeline.

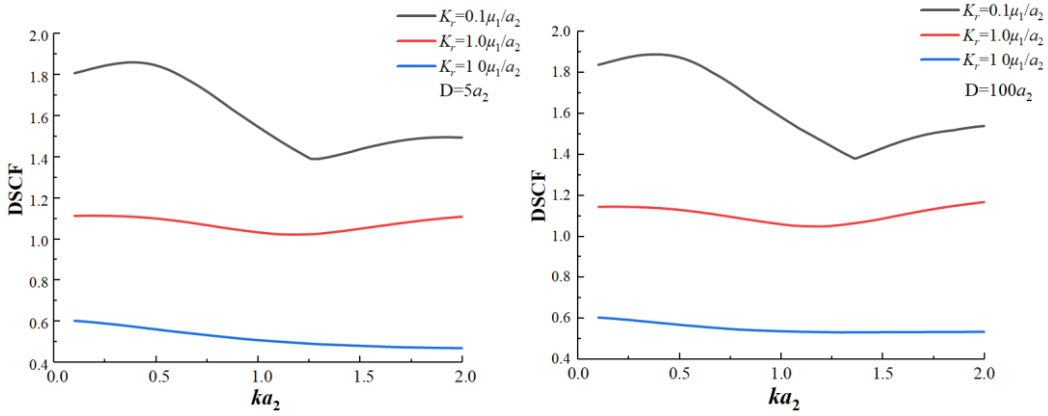

(a) D=5a2 (b) D=100a2

Figure 8: Trend curve of peak DSCF in soil with ka_2

4.4 The effect of different ka on the peak value of DSCF in the inner wall of pipeline

From Fig. 9, it can be observed that when D=5a_2 and D=100a_2, the trend of the DSCF peak curve with ka_2 is basically the same. No matter what value K_r takes, within the range of 0.1<ka_2<2.0, the peak value of DSCF gradually decreases with the increase of ka_2. From this, it can be seen that the impact of incident wave frequency f on the peak value of DSCF varies in degree under different stiffness coefficients K_r. When the stiffness coefficient K_r is small, the influence of ka_2 on its DSCF peak is relatively small. And regardless of the value of K_r, its maximum value is in the low-frequency band. The larger the interface stiffness coefficient K_r, the greater the DSCF value of the inner wall of the pipeline. This is exactly the opposite of the soil mass.

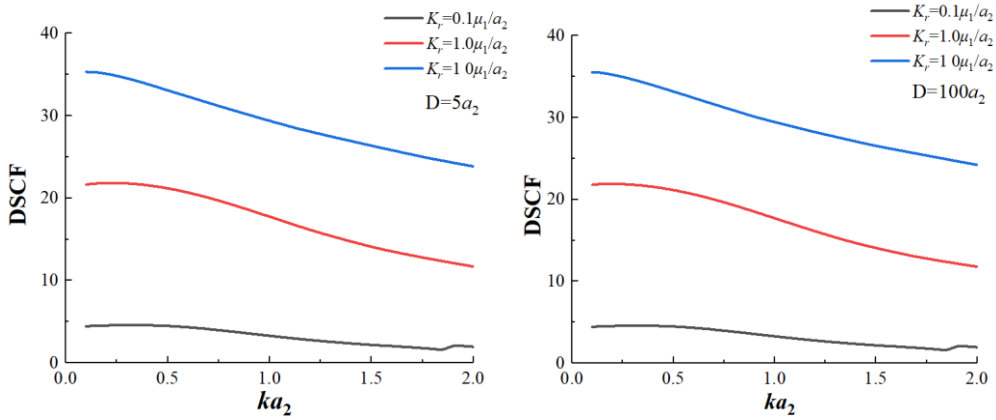

(a) D=5a2 (b) D=100a2

Figure 9: Trend curve of peak DSCF in the pipe with ka_2

5. Conclusion

This article analyzes the dynamic response of a single buried pipeline considering boundary effects under the action of cylindrical SH waves, and discusses the feasibility and accuracy of this method. The general conclusions are as follows:

Through extensive calculations and precision analysis, it can be concluded that: when a_i=0.7a, a_k=1.54a, M=N=60, and L=50, the optimal exact solution can be obtained. The calculation errors of

the soil and pipeline inner wall both meet the requirements of 10^{-10}, meeting further analysis requirements.

Through the analysis of the DSCF in the soil, it can be seen that with the variation of ka_2 and interface stiffness coefficient K_r, the maximum stress concentration coefficient (DSCF) is distributed within the range of π/3~2π/3 and 4π/3~5π/3. Therefore, the soil in this area should be a focus of attention. Under the same conditions and at the same angle θ, the larger the stiffness coefficient K_r, the smaller the DSCF value.

Compared to the soil, the DSCF value on the inner wall of the pipeline is significantly larger. And its distribution range is within the range of π/2-2 π/3 and 4 π/3-3 π/2. Therefore, under the same calculation conditions, the inner wall of the pipeline is more susceptible to damage, and the damage range is more concentrated on the side of the incident wave. Under the same conditions and at the same angle θ, the larger the stiffness coefficient K_r, the greater the DSCF value. This is exactly the opposite of the soil mass.

When $D \geq 5a_2$, the wave source distance D has little effect on the calculation of soil and pipeline inner walls, and can be treated as a plane wave. According to the analysis, there may be a threshold within the range of $a_2 < D < 5a_2$.

Acknowledgements

The study was sponsored by Hubei Provincial Natural Science Foundation (2019CFB224), Hubei Provincial Department of Education (Q201913308), Jingzhou Science and Technology Bureau (2019Z18001) and Open Research Fund of Hubei Key Laboratory of Blasting Engineering (HKLBEF202011).

References

[1] B. Wang, P. Cheng, Y. Zheng, F. Zhou, 2020. The propagation law of stress waves in loose particles. Journal of High Pressure Physics, Vol. 34, pp. 100-107.

[2] C. Yi, P. Zhang, D. Johansson, Nyberg. U, 2014. Dynamic response of a circular lined tunnel with an imperfect interface subjected to cylindrical P-waves. Computers and Geotechnics, Vol. 55, pp. 165-171.

[3] H. Liu, S. Lu, J. Sun, C. Zhou, 2021. Influence of jointed rock mass on P wave propagation. Science Technology and Engineering, Vol. 21, pp. 5929-5933.

[4] H. Xu, T. Li, J. Xu, Y. Wang, 2014. Dynamic Response of Underground Circular Lining Tunnels Subjected to Incident P Waves. Mathematical Problems in Engineering, Vol. 2014, pp. 1-11.

[5] H. Zhang, X. Du, Z. Liu, Y. Xu, G. Y, 2020. Dynamic response of double track tunnel in mountain terrain under incident surface SV wave. Engineering Mechanics, Vol. 37, pp. 77-78.

[6] H. Zhou, C. He, 2020. Propagation Law of Stress Wave and Cracks in Non-penetrating Jointed Rock Mass: A Numerical Study Based on Particle Flow Code. Geotechnical and Geological Engineering, Vol. 38, pp. 3967-3981.

[7] J. Chang, R. Yin, X. Wang, 2020. Dynamic response analysis of U-shaped tunnel in saturated soil under plane wave. Journal of Railway Engineering, Vol. 37, pp. 54-58+79.

[8] M. Dorduncu, M. K. Apalak, J. N. Reddy, 2019. Stress wave propagation in a through-thickness functionally graded adhesive layer. Journal of Adhesion Science and Technology, Vol. 33, pp. 2329-2355.

[9] N. Sun, M. Lei, Y. Zhang, G. Su, G. Huang, 2020. Research on the Influence of Weak Interlayer on the Propagation Process of Explosion Stress Wave. Vibration and Shock, Vol. 39, pp. 112-119+147.

[10] P. Jiang, H. Jiang, Y. Jiang, D. Wang, N. Li, Z. Shi, 2021. IBEM Simulation of Seismic Wave Scattering by a 3D Tunnel Mountain. Shock and Vibration, Vol. 2021, pp. 1-23.